Porphyromonas gingivalis triggers lipid metabolism disorders in atherosclerosis through the PPARγ-LXRα-ABCA1/ABCG1 signaling pathway

XUE-JING LIN[1,2*], MIN YAO[3*], WAN-YUN LIN[2], QIN YUAN[1,2], JIE ZHOU[1,2], WEN-XUAN XIA[2], YU-LEI DONG[1,2], MIAO-MIAO ZHANG[1,2], MING-WANG CUI[1,2], LIN-HAN WU[1], DIWAS SUNCHURI[4], MUHAMMAD ZIA ULLAH SHAHID[5] and ZHU-LING GUO[1,2]

[1]Key Laboratory of Emergency and Trauma of Ministry of Education, Department of Health Management Center, The First Affiliated Hospital, Hainan Medical University, Haikou, Hainan 570000, P.R. China; [2]School of Stomatology, Hainan Medical University, Haikou, Hainan 571199, P.R. China; [3]Department of Stomatology, Affiliated Children's Hospital of Nanjing Medical University, Nanjing, Jiangsu 210000, P.R. China; [4]School of International Education, Hainan Medical University, Haikou, Hainan 570000, P.R. China; [5]Frontier Medical and Dental College, Abbottabad, Khyber Pakhtunkhwa 22010, Pakistan

Received February 13, 2025; Accepted February 4, 2026

DOI: 10.3892/mmr.2026.13880

Abstract. The present study aimed to analyze the effects of *Porphyromonas gingivalis* infection on atherosclerosis caused by lipid metabolism disorders in apolipoprotein E-knockout (*ApoE*$^{-/-}$) mice. A total of 20 male *ApoE*$^{-/-}$ mice were randomly divided into two groups (n=10/group). The mice in the *ApoE*$^{-/-}$ infected group were orally inoculated with *P. gingivalis* for 6 weeks, whereas those in the *ApoE*$^{-/-}$ control group were orally administered PBS. Blood biochemistry was performed to determine the serum levels of total cholesterol (TC), triglyceride (TG), high-density lipoprotein (HDL) and low-density lipoprotein (LDL) in the mice. ELISA was used to determine the protein levels of monocyte chemotactic protein-1 (MCP-1), IL-6 and oxidized LDL (ox-LDL) in the serum of mice. In addition, a comprehensive comparison of atherosclerotic plaques and pathological changes in the liver between the *P. gingivalis*-infected group and the control group was performed. Subsequently, reverse transcription-quantitative PCR was performed to measure the expression levels of genes related to the peroxisome proliferator-activated receptor γ (PPARγ)-liver X receptor α (LXRα)-ATP-binding cassette transporter (ABC) A1/ABCG1 pathway in the liver. A total of 6 weeks after *P. gingivalis* inoculation, the levels of TC, TG, LDL, ox-LDL, IL-6 and MCP-1 in the serum of the *ApoE*$^{-/-}$ *P. gingivalis*-infected group were significantly higher compared with those in the *ApoE*$^{-/-}$ control group, whereas HDL levels were significantly lower. Furthermore, compared with in the *ApoE*$^{-/-}$ control group and the C57B6/L with *P. gingivalis* infection group, the severity of atherosclerotic plaques in the *ApoE*$^{-/-}$ group infected with *P. gingivalis* was more severe, and the vacuolar degeneration of liver cells was more pronounced, manifested by decreased levels of ABCA1, ABCG1, LXRα and PPARγ. In conclusion, *P. gingivalis* may amplify lipid metabolism disorders and aggravate the symptoms of atherosclerosis through the CD36-mediated PPARγ-LXRα-ABCA1/ABCG1 signaling pathway.

Introduction

Atherosclerotic cardiovascular disease is characterized by the thickening and hardening of the arterial wall, the formation or rupture of subendothelial plaques, and a reduction in the arterial blood supply due to stenosis or occlusion of the lumen, and is reported as the main cause of mortality worldwide (1). Periodontitis is an independent risk factor for atherosclerosis, and its molecular mechanism involves a number of inflammatory cytokines and signaling pathways. Lipoplysaccharide (LPS) from *Porphyromonas gingivalis* activates Toll-like receptor (TLR)4, inducing IL-6 release and stimulating hepatic C-reactive protein production, which subsequently upregulates vascular endothelial adhesion molecule expression; this promotes monocyte adhesion and foam cell formation, accelerating the progression of atherosclerosis (2). *P. gingivalis* is a gram-negative bacterium commonly found at sites with severe loss of periodontal tissue attachment and in deep periodontal pockets, and is associated with the progression of periodontal disease (3). *P. gingivalis* is closely related to the occurrence and development of periodontitis, as well

Correspondence to: Dr Zhu-Ling Guo, School of Stomatology, Hainan Medical University, 3 Xueyuan Road, Haikou, Hainan 571199, P.R. China
E-mail: hy0210026@hainmc.edu.cn

*Contributed equally

Key words: Porphyromonas gingivalis, lipid metabolism, atherosclerosis, CD36, peroxisome proliferator-activated receptor γ

as coronary atherosclerotic heart disease. Infection with this bacterium can, for example, lead to lipid metabolism disorders, resulting in elevated total cholesterol (TC), triglyceride (TG) and low-density lipoprotein (LDL) levels, and decreased high-density lipoprotein (HDL) levels (4,5). *P. gingivalis* promotes atherosclerosis by affecting lipid metabolism. Experimental studies have suggested that *P. gingivalis* can invade endothelial and phagocytic cells within the atheroma, leading to pathogenic changes and progression of the atheroma lesion (6,7). As the primary pathogens of chronic periodontitis, *P. gingivalis* and related toxins can enter the bloodstream through the gingival epithelium, which causes vascular endothelial dysfunction, activates blood inflammatory factors and ultimately stimulates intravascular plaque formation (8).

Peroxisome proliferator-activated receptor γ (PPARγ) has been reported to be highly expressed in the early and middle stages of human atherosclerotic lesions. In a previous study, in response to administration of 5 g/l garlic allicin, the expression levels of PPARγ in the atherosclerotic lesions of the aortic root in *ApoE*$^{-/-}$ mice were reported to be increased (9). In addition, PPARγ has been revealed to be highly expressed in RAW-derived foam cells, whereas its expression may be reduced after Dansameum extract (DSE) treatment. PPARγ is also highly expressed in the atherosclerotic lesion area of apolipoprotein E-knockout (*ApoE*$^{-/-}$) mice, with its expression further increased in the aortic plaque of mice fed a high-fat diet; by contrast, its expression can be reduced by DSE treatment (10). ATP-binding cassette transporter (ABC)A1 is the key initiator protein that mediates reverse cholesterol transport (RCT) and it has been shown that macrophage-specific overexpression of ABCA1 can reduce atherosclerotic plaque area (11). ABCG1 is a key member of the ABC superfamily, which serves a critical role in lipid metabolism. High expression of ABCG1 in macrophages reportedly reduces cholesterol accumulation and inhibits foam cell formation, thereby decelerating the progression of atherosclerotic plaques (12). Liver X receptor α (LXRα) is a key member of the nuclear receptor superfamily and is involved primarily in the regulation of cholesterol metabolism (for example, promoting the expression of ABCA1 and ABCG1 to mediate RCT) and bile acid synthesis (13). The PPARγ-LXRα-ABCA1/ABCG1 pathway regulates cholesterol efflux, whereas CD36 regulates cholesterol uptake during lipid metabolism (14). In the present study, a model of atherosclerosis and *P. gingivalis* infection was established, and the changes in lipid metabolism and inflammatory responses were observed. In addition, whether the expression of PPARγ-LXRα-ABCA1/ABCG1 and CD36 served as the mechanism of lipid metabolism disorders caused by *P. gingivalis* was investigated. As illustrated in Fig. 1, *P. gingivalis* infection may disrupt lipid homeostasis by promoting cholesterol uptake via CD36 while simultaneously inhibiting cholesterol efflux through the downregulation of the PPARγ-LXRα-ABCA1/ABCG1 pathway. This imbalance leads to lipid accumulation in macrophages and hepatocytes, thereby accelerating the progression of atherosclerosis and hepatic steatosis.

Septin 4 is a member of the GTP-binding protein family that serves an important role in preventing foam cell formation through the activation of PPARγ/LXRα signaling and subsequent enhancement of ABCA1/ABCG1 expression (15). ABCA1 expression in endothelial cells protects against atherosclerosis, and this atheroprotective effect partially contributes to enhancing ApoAI-mediated cholesterol efflux. Notably, ABCA1 is a target gene for LXR and RXR (16); therefore, treating endothelial cells with LXR and/or RXR agonists may increase ABCA1 expression (17).

However, whether *P. gingivalis* is involved in cholesterol metabolism and its mechanism remains unclear. The present study examined the effects of long-term, low-dose intraoral infection of *ApoE*$^{-/-}$ mice with *P. gingivalis* on lipid metabolism disorders, with the aim of providing further experimental evidence for the association between periodontitis and atherosclerosis.

Materials and methods

Bacterial culture. P. gingivalis (cat. no. 33277; American Type Culture Collection) was cultured in 30 g/l trypsin soybean broth supplemented with 1 g/l yeast extract, 50 mg/l heme chloride and 10 mg/l vitamin K3, inside an anaerobic tank, at 37˚C for 3 days. Subsequently, a PBS bacterial mixture with a *P. gingivalis* concentration of 10^9/ml (containing 20 g/l sodium carboxymethyl cellulose) was obtained for further use.

Mouse feeding. A total of 20 specific pathogen-free *ApoE*$^{-/-}$ male mice and 20 C57BL/6 wild-type male mice (both acquired from the Model Animal Research Center of Nanjing University, Nanjing China) were randomly selected and fed a high-fat diet (cat. no. 88137; Inotiv Inc.; 21% fat, 0.15% cholesterol, no cholate) from the age of 4 weeks. The initial body weight of *ApoE*$^{-/-}$ mice was 14.5±1.5 g, whereas that of C57BL/6 mice was 15.0±1.5 g. The mice were maintained under specific pathogen-free conditions, under a constant temperature (22±2˚C) and humidity (40-70% relative humidity), with a 12-h light/dark cycle. Both the high-fat diet and autoclaved drinking water were provided *ad libitum*. At the age of 5 weeks, each mouse was intragastrically administered ampicillin and kanamycin (2 mg each per mouse) daily for 4 days. The present study received complete ethical clearance from the ethics committee of Hainan Medical University (approval no. HYLL-2021-121; Haikou, China) and was conducted rigorously following the relevant guidelines established by the National Institutes of Health (18). Every effort was made to minimize the number of utilized mice and to mitigate any distress caused to the mice during experiments.

Experimental grouping and oral administration. *ApoE*$^{-/-}$ mice were randomly divided into the following two groups (n=10/group): The infection group and the control group. The wild-type mice were also randomly divided into an infection group and a control group (n=10/group). The sample size is consistent with that used in prior studies investigating *P. gingivalis*-induced atherosclerosis in *ApoE*$^{-/-}$ mice (19,20). From the age of 6 weeks, the abdominal area of each mouse was aseptically prepared with iodine, after which the mouse was subjected to anesthesia through an intraperitoneal (IP) injection of 1% pentobarbital sodium solution (60 mg/kg). The PBS bacterial mixture with a concentration of 10^9/ml *P. gingivalis* (containing 20 g/l sodium carboxymethyl cellulose) was smeared on the gingival region of each mouse in the infection group. The uninfected control

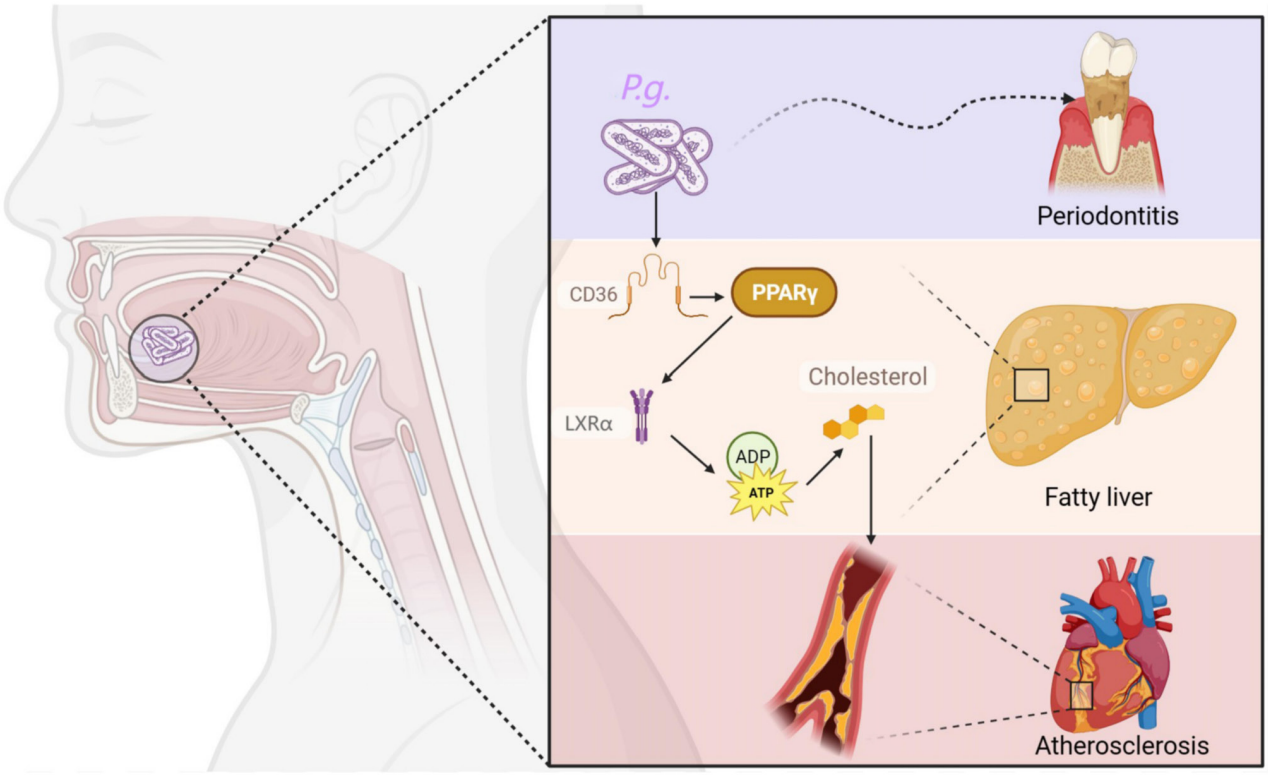

Figure 1. Mechanism through which *P.g.* causes lipid metabolism disorders and aggravates atherosclerosis via PPARγ-LXRα-ABCA1/ABCG1 and CD36. ABC, ATP-binding cassette transporter; LXRα, liver X receptor α; *P.g.*, *Porphyromonas gingivalis*; PPARγ, peroxisome proliferator-activated receptor γ.

mice received 0.1 ml PBS with 20 g/l sodium carboxymethyl cellulose in the same manner. Oral inoculation with *P. gingivalis* was performed five times per week for 6 weeks (Fig. 2). At the end of week 6, the mice were euthanized using pentobarbital overdose (200 mg/kg IP), followed by cervical dislocation and collection of the mandibles. The remaining experimental mice (10 *ApoE*$^{-/-}$ type and 10 wild-type) were sacrificed at the 12th week for sample collection.

Microcomputed tomography (micro-CT) analysis. The mandibles were fixed in 10% buffered formalin for 24 h at 4˚C, followed by storage in PBS at 4˚C prior to micro-CT (USPECT-II/CT; MILabs B.V.) analysis. The mandibles of mice were imaged using a voxel size of 25 μm, scan settings of 70 kVp, 114 μA and 0.5 mm aluminum filter, and an integration time of 500 msec. A 3D construction was created using Avizo software (version 9.1; Thermo Fisher Scientific, Inc.).

Determination of serum lipid and inflammatory factor levels. At the ages of 6 and 12 weeks, the weights of all mice were recorded, and each group of mice was subjected to pentobarbital overdose (200 mg/kg IP), followed by cervical dislocation for euthanasia. In week 6, 10 *ApoE*$^{-/-}$ male mice and 10 C57BL/6 wild-type male mice were sacrificed, and in week 12, 10 *ApoE*$^{-/-}$ male mice and 10 C57BL/6 wild-type male mice were sacrificed; within each group of mice, five were from the infection group and five were from the control group. After euthanasia, the height of the alveolar bone of each mouse was measured and blood samples (0.4 ml) were collected from the mouse eyeballs via the retro-orbital vein and anticoagulated using heparin. After centrifugation at 4˚C for 10 min at 1,960 x g, the serum from the blood samples was collected and stored at -70˚C for further use in the measurement of the serum levels of TC (cat. no. 100051013), TG (cat. no. 100051014), HDL (cat. no. 100020235) and LDL (cat. no. 100020245) (all from Zhongsheng Beikong Biotechnology Co., Ltd.) using blood biochemical methods. In addition, the serum levels of oxidized LDL (ox-LDL; cat. no. CSB-E07933m), IL-6 (cat. no. CSB-E04639m) and monocyte chemotactic protein-1 (MCP-1; cat. no. CSB- E07430m) (all from Cusabio Technology, LLC) were determined using ELISA.

Preparation of periodontal tissues, liver and aorta samples. Collection of atherosclerotic plaques: The heart and aorta were perfused slowly with normal saline at 4˚C through the left ventricle for 10 min, and the aorta (including the aortic arch, thoracic aorta and abdominal aorta) was identified. The connective tissue around the artery was stripped, and the integrity of its bifurcation to the iliac bone was ensured. The isolated mouse aorta was washed with normal saline at 4˚C, and the excess liquid was dried using filter paper and immediately placed into liquid nitrogen for freezing, and preservation at -80˚C. Meanwhile, the liver was removed for further use. The levels of PPARγ (cat. no. CSB-E08625m; Cusabio Technology, LLC), ABCA1 (cat. no. LS-F21311; LS Bio; Vector Laboratories, Inc.) and ABCG1 (cat. no. ASET-2063; Ace Therapeutics), and LXRα (cat. no. MBS2020587; MyBioSource, Inc.), in periodontal tissues and plaque were detected by ELISA. The specific procedure was performed according to the corresponding kit instructions. After collection, the liver samples were washed with normal saline and fixed with 40 g/l neutral polycarboxylic acid at 4˚C for 24 h. Paraffin-embedded sections (4-5 μm) were subjected

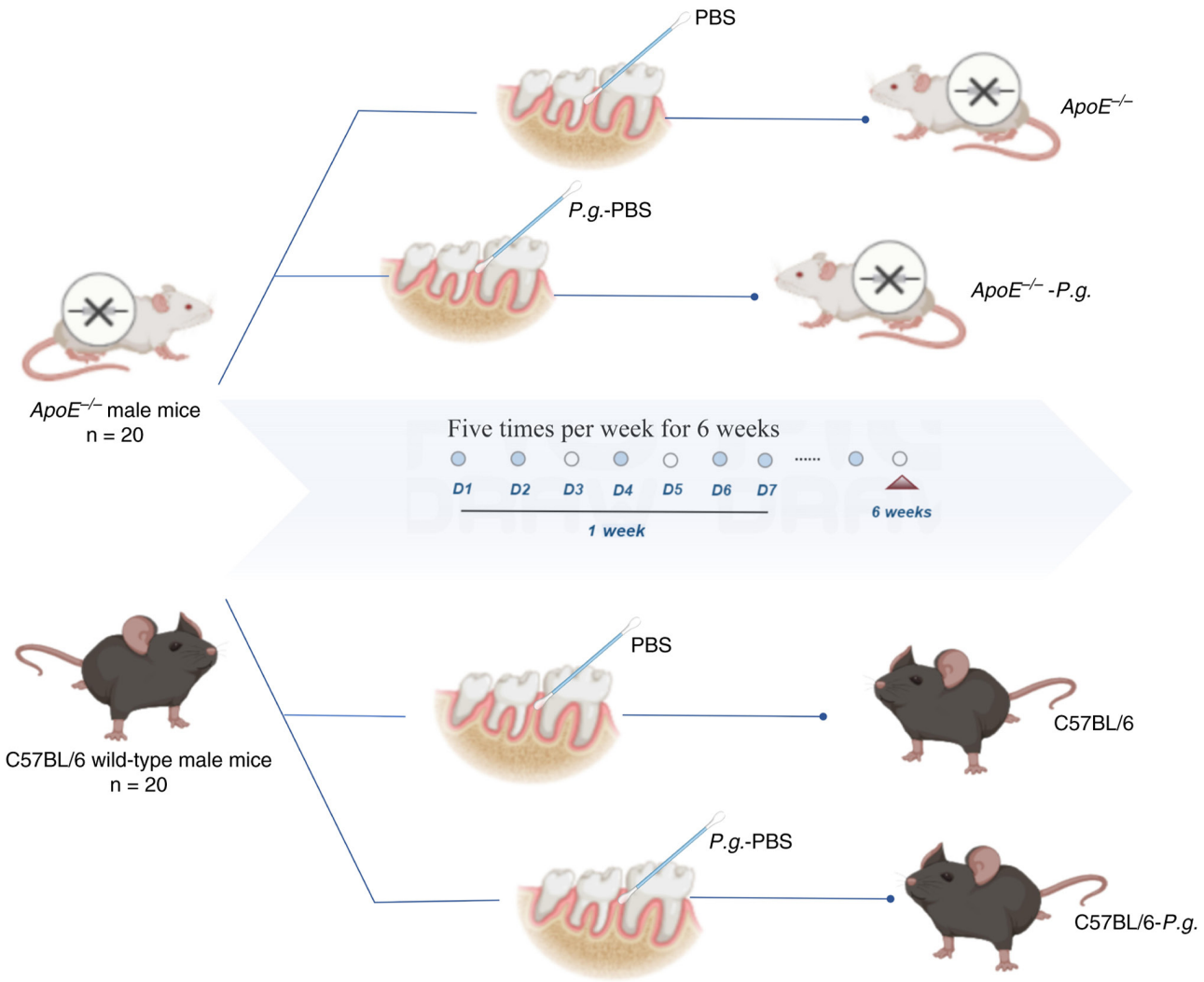

Figure 2. Establishment of the mouse model. *ApoE*$^{-/-}$, apolipoprotein E-knockout; *P.g.*, *Porphyromonas gingivalis*.

to hematoxylin and eosin (H&E) staining at room temperature (20-25˚C) and observed under a bright-field microscope. Collection of periodontal tissues: After the mice were sacrificed and fully perfused, the gingival and periodontal ligament soft tissues surrounding the maxillary molars were cut off, washed, frozen quickly and stored at -80˚C for later use in ELISA.

Oil red O staining of atherosclerotic plaques. The aortic tissues were first embedded with frozen embedding agent OCT (Thermo Fisher Scientific, Inc.) and were then sliced across the aorta at a thickness of 5 μm from the proximal end to the distal end. The sections were dried at room temperature and soaked in 60% isopropanol for 5 min. Dip dyeing with oil red O dye solution was performed for 30 min in the dark at room temperature. Under a light microscope, the area stained with oil red O was defined as the atherosclerotic lesion area.

Detection of the mRNA expression levels of ABCA1, ABCG1, PPARγ, LXRα and CD36 in the liver. Total RNA was extracted from mouse liver tissue using TRIzol® reagent (cat. no. 15596026; Invitrogen; Thermo Fisher Scientific, Inc.), purified and reverse transcribed into cDNA using the PrimeScript™ RT reagent kit (cat. no. RR037A; Takara Bio, Inc.) according to the manufacturer's protocol. The RT reaction was performed at 37˚C for 15 min, followed by heat inactivation at 85˚C for 5 sec. The cDNA was stored at -20˚C until further use. The mRNA expression levels of *CD36, ABCA1, ABCG1, PPARγ and LXRα* were determined using qPCR (StepOne; Applied Biosystems; Thermo Fisher Scientific, Inc.) with TB Green™ Premix Ex Taq™ II (Tli RNaseH Plus) (cat. no. RR820A; Takara Bio, Inc.) and were normalized to the levels of GAPDH. Primer sequence information is presented in Table I. The qPCR thermocycling conditions were as follows: Pre-denaturation at 95˚C for 10 sec, followed by 40 cycles of heating at 95˚C for 5 sec and 62˚C for 20 sec. The product was slowly and evenly heated from 50˚C to 95˚C, and the melting product curve was automatically drawn using the qPCR equipment. The Cq value was determined using a computer program, the $2^{-\Delta\Delta Cq}$ value serves as the expression level of the target gene mRNA, and the software automatically generated the amplification and melting curves and calculated the relative mRNA expression levels (21,22).

Detection of oxidative stress molecules. Malondialdehyde (MDA) levels were determined as follows: The liver was placed into a mortar in an ice bath, and 2 ml 10% trichloroacetic acid

Table I. Sequences of the primers used for quantitative PCR.

Gene	Primer sequence, 5'-3'
CD36	F: TGATTAACGGGACAGACGGAGAC
	R: ACGTTCTCAAAGCTGCTGAAAGTG
ABCA1	F: AAAACCGCAGACATCCTTCAG
	R: CATACCGAAACTCGTTCACCC
ABCG1	F: ATACAGGGGAAAGGTCTCCAA
	R: CCCCCGAGGTCTCTCTTATAGT
PPARγ	F: GTACTGTCGGTTTCAGAAGTGCC
	R: ATCTCCGCCAACAGCTTCTCCT
LXRα	F: GTTATAACCGGGAAGACTTTGCCA
	R: GCCTCTCTACCTGGAGCTGGT
GAPDH	F: CATCACTGCCACCCAGAAGACTG
	R: ATGCCAGTGAGCTTCCCGTTCAG

ABC, ATP-binding cassette transporter; LXRα, liver X receptor α; PPARγ, peroxisome proliferator-activated receptor γ.

(TCA; cat. no. T0699; Sigma-Aldrich; Merck KGaA) and a small amount of quartz sand were added to it. The mixture was then crushed until it was homogenized and was subsequently centrifuged at 12,000 x g at 4˚C for 15 min, after which the supernatants were collected. The supernatant was further centrifuged at 5,000 x g for 10 min at 4˚C, and then adjusted to a volume of 1.5 ml with 10% TCA; the control group consisted of 1.5 ml 10% TCA in the absence of a tissue sample. An equal volume of 0.5% thiobarbituric acid (cat. no. T5500; Sigma-Aldrich; Merck KGaA) solution was added, and the mixture was incubated in a boiling water bath for 30 min. After rapid cooling, the mixture was centrifuged at 3,000 x g for 10 min at room temperature. Again, the mixture was allowed to react in a boiling water bath for 30 min, and then cooled quickly and centrifuged at 3,000 x g at room temperature for 10 min. The absorbance of the supernatant was measured at 532, 450 and 600 nm.

Superoxide dismutase (SOD) was detected using a kit (cat. no. 706002; Cayman Chemical Company), as follows: Organ homogenates from the liver were prepared in cold Tris buffer (5 mmol/l, containing 2 mmol/l EDTA, pH 7.4), utilizing a homogenizer with a 1,500 rotatory speed of piston/min. The homogenates were then centrifuged at 10,000 x g for 10 min at 4˚C, and the supernatants were collected. A total of 0.2 ml supernatant obtained after centrifugation (1,500 x g at 4˚C for 10 min, followed by 10,000 x g at 4˚C for 15 min) of 10% liver homogenate was added to the reaction system containing xanthine oxidase, nitroblue tetrazolium and xanthine in phosphate buffer (pH 7.8) to form the reaction mixture. The enzyme reaction was initiated by adding 0.2 ml NADH (780 μmol/l) and stopped precisely after 1 min by adding 1 ml glacial acetic acid. The amount of chromogen formed was measured at 560 nm. SOD activity was calculated from the percentage inhibition of formazan formation, with one unit defined as the amount of enzyme causing 50% inhibition of the color development.

To determine the glutathione (GSH) content, a kit (cat. no. 703002; Cayman Chemical Company) was used. Briefly, 1 ml liver homogenate supernatant was mixed with 3 ml 0.25 mol/l Tris-HCl buffer (pH 8.0), and the mixture was shaken well. Subsequently, 1 ml 3% formaldehyde was added, and the mixture was shaken again. After being incubated at room temperature for 2 and 60 min, 1 ml was immediately collected, and 5 ml 5,5'-Dithiobis(2-nitrobenzoic acid) analytical solution was added to it in a water bath at a constant temperature of 25˚C. After shaking well, the samples were allowed to stand for 5 min, after which the absorbance was measured immediately at a wavelength of 412 nm. The difference between absorbance value at the 2-min time point and the absorbance value at the 60-min time point was calculated and substituted into the regression equation to calculate the corresponding GSH concentration; the maximum error did not exceed 6%.

Statistical analysis. Data are presented as the mean ± SEM and each experimental procedure was conducted at least three times. Statistical analyses were carried out using SPSS software (version 22.0; IBM Corp.). Data were analyzed using one-way ANOVA followed by Tukey's or Dunnett's post hoc tests for normally distributed data, or Kruskal-Wallis test followed by Dunn's post hoc test for non-normally distributed data. Normality was assessed using the Shapiro-Wilk test. $P<0.05$ was considered to indicate a statistically significant difference.

Results

Comparison of the weights and alveolar bone heights of mice. There was no significant difference in weight between the *ApoE*$^{-/-}$ infected group and the *ApoE*$^{-/-}$ control group at the ages of 6 and 12 weeks ($P>0.05$; Table II). In addition, no significant difference in weight was observed between the wild-type infected group and the wild-type control group at the ages of 6 and 12 weeks ($P>0.05$; Table II). Alveolar bone loss in response to *P. gingivalis* oral infection in both groups was determined using micro-CT. Micro-CT analysis of the mandibles revealed obvious alveolar bone resorption in both the *P. gingivalis*-infected C57BL/6 group (Fig. 3B) and the *P. gingivalis*-infected *ApoE*$^{-/-}$ group (Fig. 3D) compared with in their respective uninfected controls (Fig. 3A and C). In addition, the levels of PPARγ, LXRα, ABCA1 and ABCG1 in the periodontal tissues of the *ApoE*$^{-/-}$ infected group were lower than those in the *ApoE*$^{-/-}$ control group and the C57BL/6-*P.g.* group ($P<0.05$; Fig. 3E-H).

Serum levels of MCP-1 and IL-6. IL-6 has been shown to upregulate the expression of cell adhesion molecules (such as CD54, CD102 and CD31) and potentiate vascular permeability, whereas MCP-1 can induce monocytes to penetrate the arterial wall, which leads to sustained loss of endothelial barrier function (23,24). In order to confirm whether *P. gingivalis* infection could induce an inflammatory reaction, serum MCP-1 and IL-6 levels in *ApoE*$^{-/-}$ and wild-type mice were measured. As shown in Fig. 4C and D, the serum MCP-1 and IL-6 levels in the *ApoE*$^{-/-}$ and wild-type infected groups were significantly greater than those in the comparable control groups, indicating that *P. gingivalis* infection may trigger an effective systemic inflammatory response in the mice. Therefore, the effects of PPARγ-LXRα-ABCA1/ABCG1 and CD36 signaling on the development of atherosclerosis induced by *P. gingivalis* were investigated.

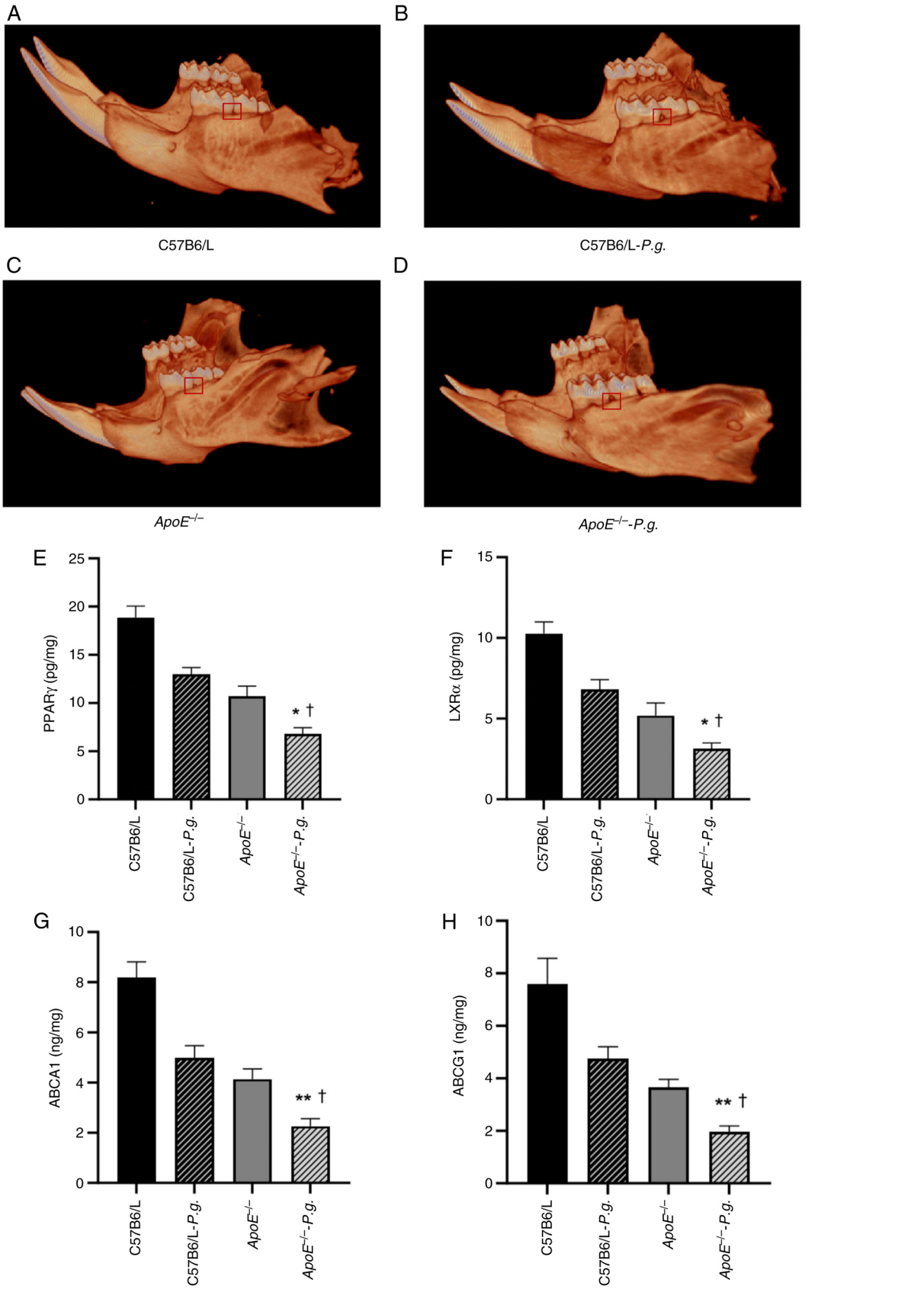

Figure 3. Effects of *P.g*. infection on the periodontium in mice. (A) C57B6/L: No notable alveolar bone resorption was observed. (B) C57B6/L-*P.g*.: Compared with the C57B6/L group, there was marked alveolar bone resorption. (C) *ApoE*$^{-/-}$ control group: Slight alveolar bone resorption was detected. (D) *ApoE*$^{-/-}$-*P.g*. infection group: Compared with the *ApoE*$^{-/-}$ control group, alveolar bone resorption was markedly aggravated. Scale bars: 700 μm. The protein levels of (E) PPARγ, (F) LXRα, (G) ABCA1 and (H) ABCG1 in the periodontal tissues in the *ApoE*$^{-/-}$ infected group were lower than those in the *ApoE*$^{-/-}$ control group and the wild-type infected group. Data are presented as the mean ± SEM (n=5). *P<0.05, **P<0.01 vs. *ApoE*$^{-/-}$; †P<0.05 vs. C57B6/L-*P.g*. Data for (E-H) were not normally distributed (Shapiro-Wilk test, P<0.05) and were analyzed using the Kruskal-Wallis test followed by Dunn's post hoc test. ABC, ATP-binding cassette transporter; *ApoE*$^{-/-}$, apolipoprotein E-knockout; LXRα, liver X receptor α; *P.g*., *Porphyromonas gingivalis*; PPARγ, peroxisome proliferator-activated receptor γ.

Table II. Weights of C57B6/L and *ApoE*$^{-/-}$ mice at 6 and 12 weeks of age (n=5/group).

	Weight, g			
Age	*ApoE*$^{-/-}$	*ApoE*$^{-/-}$-*P.g*.	C57B6/L	C57B6/L-*P.g*.
6 weeks	23.32±2.23	23.48±0.96	26.27±0.60	26.97±0.63
12 weeks	24.67±2.66	23.50±1.33	28.23±1.19	27.05±1.46

Data are presented as the mean ± SEM (n=5). *ApoE*$^{-/-}$, apolipoprotein E-knockout; *P.g*., *Porphyromonas gingivalis*. No significant difference in weight was observed among the groups.

Table III. Oxidative stress molecules in the livers of C57BL6/6 and *ApoE*$^{-/-}$ mice (n=5/group).

Parameter	*ApoE*$^{-/-}$	*ApoE*$^{-/-}$-*P.g*.	C57B6/L	C57B6/L-*P.g*.
GSH, μmol/gprot	6.74±0.35	5.21±0.33^{a}	8.62±0.41	8.33±0.25
SOD, μ/mgprot	3.12±0.21	2.30±0.36^{b}	3.92±0.20	3.62±0.36
MDA, μmol/gprot	2.76±0.44	3.55±0.39^{b}	1.86±0.20	1.90±0.19

Data are presented as the mean ± SEM (n=5). ^{a}P<0.001, ^{b}P<0.01 vs. *ApoE*$^{-/-}$. *ApoE*$^{-/-}$, apolipoprotein E-knockout; GSH, glutathione; MDA, malondialdehyde; SOD, superoxide dismutase; *P.g*., *Porphyromonas gingivalis*.

Effects of P. gingivalis on blood lipid metabolism in atherosclerotic plaques in mice. As shown in Fig. 4A and B, the results of the histological analysis of the Oil Red O-stained sections revealed irregularly elevated atherosclerotic plaques along the intimal surface in both *ApoE*$^{-/-}$ control and *P. gingivalis*-infected groups. Notably, the plaques in the infected group were larger, exhibited greater protrusion into the intima, and led to a more pronounced compression of the underlying medial layer. The plaque was further elevated by the rupturing of new blood vessels within the plaque, leading to hematoma formation. In addition, *P. gingivalis* infection inhibited the levels of PPARγ, LXRα, ABCA1 and ABCG1 in plaque; this was manifested by the lower levels of PPARγ, LXRα, ABCA1 and ABCG1 in the *ApoE*$^{-/-}$ infected group compared with in the *ApoE*$^{-/-}$ control group, and the levels in the *ApoE*$^{-/-}$ infected group also lower than those in the wild-type infected group (P<0.05) (Fig. 4J-M). Next, the effects of *P. gingivalis* on lipid metabolism were evaluated by determining the levels of HDL, LDL, ox-LDL, TG and TC. As shown in Fig. 4E-I, there was no significant difference in these five blood lipid indices between the wild-type control group and the wild-type infected group, indicating that *P. gingivalis* infection cannot directly cause lipid metabolism disorders. Notably, the levels of LDL, ox-LDL, TC and TG in the serum of the *ApoE*$^{-/-}$ infected group were significantly greater compared with those in the serum of the *ApoE*$^{-/-}$ control group, whereas the HDL levels were significantly lower (P<0.05). These results revealed that *P. gingivalis* could exacerbate lipid metabolism disorders.

Effects of oral infection with P. gingivalis on liver hepatocytes. As shown in Fig. 5A-D, the images of the H&E-stained sections revealed that compared with in the C57B6/L group, *P. gingivalis* infection in the wild-type group resulted in a mild increase in hepatocyte volume with a small number of lipid droplets. Furthermore, compared with in the *P. gingivalis*-infected C57B6/L group, the *ApoE*$^{-/-}$ group showed moderately increased hepatocyte volume with increased lipid droplets, whereas the *ApoE*$^{-/-}$ infection group displayed the most notable increase in hepatocyte volume, with numerous lipid droplets fusing into large vacuoles and nuclei displaced to the cell periphery, presenting obvious macrovesicular steatosis. These results indicated that *P. gingivalis* infection may exacerbate hepatocyte steatosis in *ApoE*$^{-/-}$ mice. Furthermore, the effects of *P. gingivalis* infection on the expression of *PPARγ*, *LXRα*, *ABCA1*, *ABCG1* and *CD36* in the liver were measured using RT-qPCR. As shown in Fig. 5E-H, compared with in the *ApoE*$^{-/-}$ control group, there was no significant difference in the mRNA levels of ABCG1 in the livers of mice in the *ApoE*$^{-/-}$ *P. gingivalis* infection group (P>0.05), whereas the levels of ABCA1, PPARγ and LXRα were significantly decreased (P<0.05). In addition, the mRNA levels of CD36 were significantly increased in the *ApoE*$^{-/-}$ infected group compared with those in the *ApoE*$^{-/-}$ control group (P<0.05; Fig. 5I). Compared with in the wild-type control group, the levels of ABCA1 in the wild-type infected group were decreased, whereas the levels of ABCG1 and PPARγ were increased (P<0.05), and there was no significant difference in the levels of CD36 and LXRα between these two groups (P>0.05).

Effects of P. gingivalis on the levels of oxidative stress molecules. Compared with those in the *ApoE*$^{-/-}$ control group, the levels of GSH and SOD were significantly lower in the livers of the *ApoE*$^{-/-}$ infected group mice, whereas the levels of MDA were significantly greater (P<0.05; Table III). By contrast, there was no significant difference in the levels of GSH, SOD and MDA between the two groups of C57BL/6 wild-type mice (P>0.05; Table III).

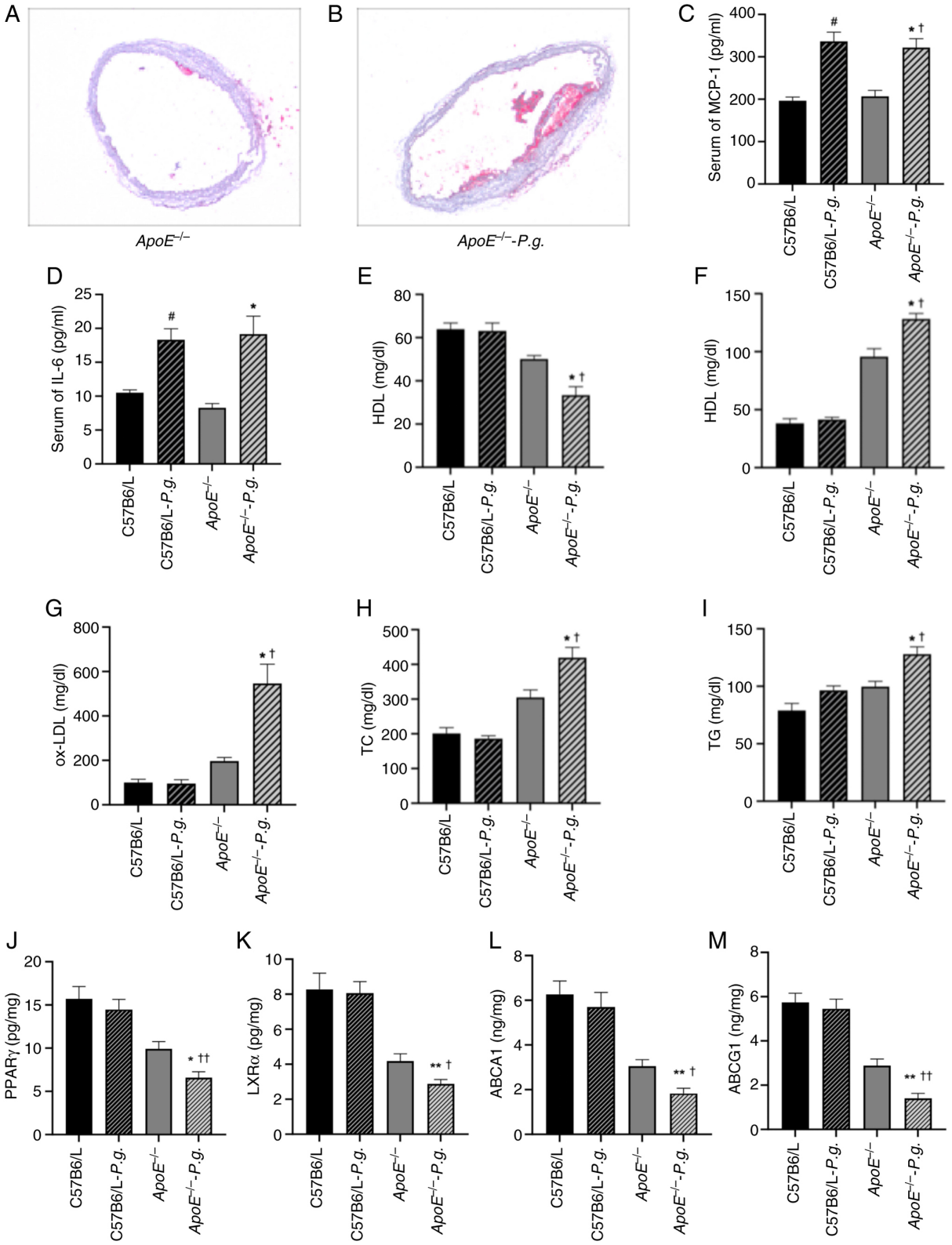

Figure 4. Effects of *P.g*. on blood lipid metabolism and atherosclerotic plaques in mice. (A) Oil red O staining of aortic root cross-sections from *ApoE*$^{-/-}$ mice (magnification, x200). The image shows scattered lipid deposits (red-stained areas) in the aortic wall in the absence of *P.G*. infection, characteristic of early atherosclerotic lesions. (B) Oil red O staining of aortic root cross-sections from *ApoE*$^{-/-}$ mice following *P.g*. infection (magnification, x200). Compared with in the control, the atherosclerotic plaque area was markedly increased, with more extensive and densely distributed red-stained regions indicating enhanced lipid deposition. Serum levels of (C) MCP-1 and (D) IL-6 were determined using ELISA. Levels of (E) HDL, (F) LDL, (H) TC and (I) TG were determined using blood biochemical methods. (G) Serum levels of ox-LDL were determined using ELISA. Levels of (J) PPARγ, (K) LXRα, (L) ABCA1 and (M) ABCG1 were determined using ELISA. Data are presented as the mean ± SEM (n=5). *P<0.05, **P<0.01 vs. *ApoE*$^{-/-}$; †P<0.05, ††P<0.01 vs. C57B6/L-*P.g*; $^{\#}$P<0.05 vs. C57B6/L. Data for (C, D, G and J-M) were not normally distributed (Shapiro-Wilk test, P<0.05) and were analyzed using the Kruskal-Wallis test followed by Dunn's post hoc test. Data for (E, F, H and I) were normally distributed and analyzed using one-way ANOVA followed by Tukey's or Dunnett's post hoc test. ABC, ATP-binding cassette transporter; *ApoE*$^{-/-}$, apolipoprotein E-knockout; HDL, high-density lipoprotein; LDL, low-density lipoprotein; LXRα, liver X receptor α; MCP-1, monocyte chemotactic protein-1; ox-LDL, oxidized LDL; *P.g*., *Porphyromonas gingivalis*; PPARγ, peroxisome proliferator-activated receptor γ; TC, total cholesterol; TG, triglyceride.

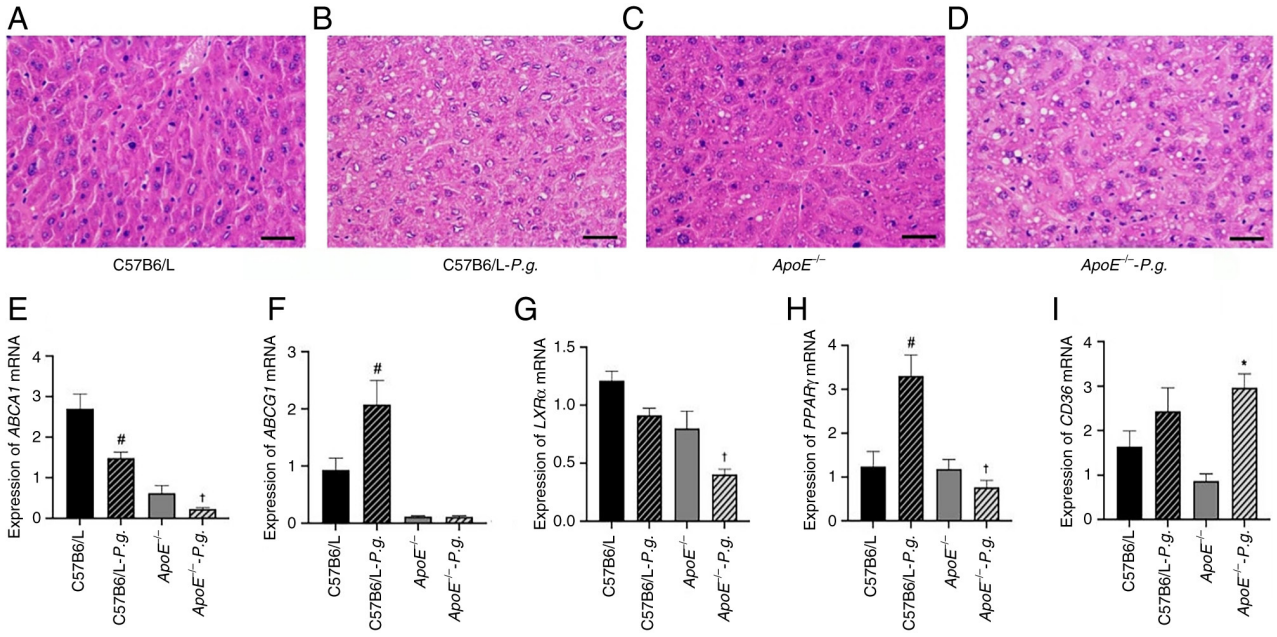

Figure 5. Effects of *P.g.* infection on lipid metabolism disorders and liver cells. (A-D) Representative images of hematoxylin and eosin staining in liver hepatocytes (magnification, x400). (A) Liver cells in the C57B6/L group had a regular shape, uniform size and uniform cytoplasm. There was no obvious lipid droplet deposition. The liver lobule structure was intact, and no hepatic cell fatty degeneration or morphological abnormalities were observed. (B) Compared with in the C57B6/L group, the liver cell volume in the C57B6/L-*P.g.* group was slightly enlarged. A few scattered small lipid droplets can be seen in the cytoplasm, without obvious lipid droplet fusion or nuclear displacement. There was a slight change of hepatic cell fatty degeneration. (C) Liver cell volume in the *ApoE*$^{-/-}$ group was moderately enlarged. The number of lipid droplets in the cytoplasm was more than that in the C57B6/L-*P.g.* group. Some lipid droplets showed small-scale fusion, and a few liver cells showed a slight displacement of the nucleus, presenting moderate characteristics of hepatic cell fatty degeneration. (D) Compared with in the *ApoE*$^{-/-}$ control group, the liver cell volume in the *ApoE*$^{-/-}$*-P.g.* group was markedly enlarged. A large number of lipid droplets in the cytoplasm fused to form large vacuoles, occupying most of the cytoplasm. The nucleus was compressed to the edge of the cell, presenting typical large vacuolar fatty degeneration. The degree of hepatic cell fatty degeneration was severe. Effects of *P.g.* on the mRNA expression levels of (E) *ABCA1*, (F) *ABCG1*, (G) *LXRα*, (H) *PPARγ* and (I) *CD36* in the liver were determined using reverse transcription-quantitative PCR. Data for (E-I) were not normally distributed (Shapiro-Wilk test, P<0.05) and were analyzed using the Kruskal-Wallis test followed by Dunn's post hoc test. Data are presented as the mean ± SEM (n=5). $^{\#}$P<0.05 vs. C57B6/L; *P<0.05 vs. *ApoE*$^{-/-}$; †P<0.05 vs. C57B6/L-*P.g.* ABC, ATP-binding cassette transporter; *ApoE*$^{-/-}$, apolipoprotein E-knockout; LXRα, liver X receptor α; *P.g.*, *Porphyromonas gingivalis*; PPARγ, peroxisome proliferator-activated receptor γ.

Discussion

Atherosclerotic plaque initiation and progression are characterized by massive deposition and accumulation of lipid-loaded macrophages within arterial walls (12). Numerous studies have shown that the pathogenesis of atherosclerosis mainly involves inflammation, with bacteria serving the role of inflammatory initiators in this process (25,26). Periodontal pathogens and their products have been reported to interfere with lipid distribution and metabolism in macrophages (27,28). Any disturbance in the cholesterol-handling machinery in macrophages, particularly the impairment of their cholesterol efflux capacity, is closely associated with foam cell formation, an aberrant serum lipid profile and reduced RCT efficiency, all of which contribute to the development of atherogenesis (29). In the present study, the effects of *P. gingivalis* infection on atheromatous plaque formation in *ApoE*$^{-/-}$ mice were investigated, and the involvement of the PPARγ-LXRα-ABCA1/ABCG1 and CD36 signaling pathways as potential mechanisms underlying the *P. gingivalis*-induced lipid metabolism disorders was explored. For this, male *ApoE*$^{-/-}$ mice were fed a high-fat diet and were then injected with ampicillin and kanamycin at the age of 5 weeks to control for biological variables that may interfere with the establishment of a *P. gingivalis* infection model. According to previous studies, mice were treated with ampicillin and kanamycin (2 mg/mouse) daily for 4 days to suppress the native oral flora and promote subsequent colonization of *P. gingivalis* (30). An oral bacterial mixture was used to establish an atherosclerosis model of *P. gingivalis* infection. A comparison of the alveolar bone height and aortic plaque area between the infected and control groups confirmed that *P. gingivalis* infection promoted the formation of atherosclerotic plaques and decreased the alveolar bone height. In addition, *P. gingivalis* infection led to an imbalance of oxidation and antioxidation. Finally, it was revealed that PPARγ-LXRα-ABCA1/ABCG1 and CD36 signaling pathways may be involved in *P. gingivalis*-induced lipid metabolism disorders in *ApoE*$^{-/-}$ mice, which further exacerbated atherosclerosis progression. The results indicated that in the liver samples of *ApoE*$^{-/-}$ mice infected with *P. gingivalis*, the levels of the core molecules of the PPARγ-LXRα-ABCA1/ABCG1 pathway were abnormally downregulated, whereas the levels of the key molecule for lipid uptake, CD36, were significantly upregulated. Together, CD36 upregulation and downregulation of the PPARγ-LXRα-ABCA1/ABCG1 pathway may mediate an imbalance between excessive lipid uptake and impaired cholesterol efflux in mice, leading to severe lipid metabolism disorders characterized by elevated serum TC, TG, LDL and ox-LDL, and decreased HDL. This could further aggravate the pathological damage of atherosclerotic plaques in the mice, and simultaneously cause foamy fatty degeneration in the liver, resulting in severe damage to liver lipid metabolism.

In chronic periodontitis, virulence factors, including LPS, fimbriae and outer membrane vesicles, continue to enter the circulatory system, increasing the number of inflammatory cells and the released cytokines. Notably, IL-6 is abundantly released during the development of atherosclerosis. Moreover, an established connection exists among IL-6 levels, endothelial dysfunction and subclinical atherosclerosis, and multiple studies have reported that IL-6 signaling serves a role in atherothrombosis (23,31). Smooth muscle cells in plaques induce MCP-1, which promotes the inflammatory response to blood lipids (32). MCP-1 has an important role in the process of monocyte accumulation at the lesion site of atherosclerosis and entry into the vascular wall through endothelial cells. Other studies have reported similar results: *P. gingivalis* infection has been shown to accelerate atherosclerotic plaque development in *ApoE*$^{-/-}$ mice, which was revealed to be associated with increased serum levels of the atherosclerotic factors MCP-1 and IL-6 (33). The micro-CT results in the current study showed that *P. gingivalis* infection exacerbated alveolar bone resorption, and the ELISA results revealed that the levels of IL-6, MCP-1, TC, TG and LDL were significantly increased, whereas the levels of HDL were decreased in the serum of *ApoE*$^{-/-}$ mice after stimulation with *P. gingivalis,* which aggravated the inflammatory response. These findings further confirmed that *P. gingivalis* infection stimulated the levels of IL-6 and MCP-1, and aggravated the atherosclerotic process in *ApoE*$^{-/-}$ mice.

The accumulation of free cholesterol in the liver mitochondria causes mitochondrial dysfunction, activating the unfolded protein response of the endoplasmic reticulum, and leading to endoplasmic reticulum stress and hepatocyte apoptosis (34). H&E staining of the liver tissue samples from mice in the present study revealed an increase in hepatocyte volume and steatosis in the *ApoE*$^{-/-}$ mice infected with *P. gingivalis*. Lipid deposition can also induce oxidative stress injury, and these two together accelerate the formation of lipid peroxidation products (35). By contrast, SOD is considered to have anti-atherosclerosis effects. Studies have shown that carotid intimal-medial thickness values are positively associated serum small dense LDL (sdLDL) and MDA levels, and are negatively associated with SOD activity, which is also in line with the protective mechanism of oxidative damage and antioxidation (36,37). In the present study, the levels of GSH and SOD in the livers of *ApoE*$^{-/-}$ mice infected with *P. gingivalis* were significantly lower than those in non-infected *ApoE*$^{-/-}$ mice, whereas the levels of MDA were significantly increased. Some studies have shown that changes in the protein levels of SOD are not significant, but SOD activity still varies significantly across disease states (38,39). LDL is transformed into modified LDL under oxidative stress. Therefore, a study of the oxidative stress response in infected mice can further reveal the possible mechanism of *P. gingivalis*-induced atherosclerosis.

The levels of TC, TG, LDL and HDL are commonly used to evaluate the blood lipid levels of patients. TC is the sum of free cholesterol and cholesterol esters in the blood, which are synthesized and stored in the liver. Serum TC, therefore, serves as an indicator of lipid metabolism in patients. TG primarily serves as an energy storage molecule. LDL is positively associated with the incidence of atherosclerosis and is easily modified by reactive oxygen species to form ox-LDL, which can activate endothelial cells. HDL is an anti-atherosclerosis lipoprotein. With a decrease in plasma HDL levels, cholesterol metabolism becomes dysregulated; HDL can accept excessive cholesterol in the body and transport cholesterol from damaged plaques to the liver (a process known as RCT) (1,11). The liver inflammatory response can increase the levels of proinflammatory substances in systemic blood, which then exacerbates the development of atherosclerosis (40). Few studies have explored the effects of metabolic inflammation on lipid metabolism. For example, some experiments have shown that the endothelial protective function of HDL deteriorates sharply in patients with periodontitis (41). The inflammatory response also promotes the oxidation of LDL to ox-LDL and the formation of atherosclerotic plaques (42). In the present study, the serum levels of LDL, ox-LDL, TG and TC were significantly increased, whereas HDL levels were significantly decreased in *ApoE*$^{-/-}$ mice infected with *P. gingivalis* compared with those in the uninfected *ApoE*$^{-/-}$ group. Additionally, the plaques that appeared on the intimal surface in the *P. gingivalis*-infected *ApoE*$^{-/-}$ group were larger than those in the uninfected *ApoE*$^{-/-}$ group and protruded into the intimal surface, more deeply compressing the medial membrane. Different *P. gingivalis* strains vary in their virulence, adherence ability, invasion and survivability. Therefore, the variability in the effects of *P. gingivalis* on lipid metabolism needs to be confirmed by further studies. The present study indicated that inflammatory reactions and lipid metabolism disorders are important pathogenic mechanisms underlying atherosclerosis. The interrelationship between these two factors and the order of their effects after *P. gingivalis* infection need to be further investigated and confirmed in future studies investigating the progression of atherosclerosis.

The intake of modified LDL mediated by CD36 is an important mechanism of atherosclerosis induction by *P. gingivalis*. CD36 is a pattern recognition receptor that binds to multiple ionic ligands on both pathogens and host cells (43). CD36 effectively regulates lipid metabolism by promoting HDL synthesis in macrophages, participating in cholesterol efflux, and upregulating ABCA1 expression (44). When CD36 uptake of ox-LDL is unrestricted, macrophages transform into foam cells when intracellular lipid accumulation exceeds the ability of ABCA1 and ABCG1 to excrete excess cholesterol. The RT-qPCR results of the present study indicated that the expression levels of CD36 were increased in *ApoE*$^{-/-}$ infected group, whereas no significant change was observed in wild-type mice following infection. This finding is consistent with those reported in previous studies. In a previous study, after periodontal inflammation was induced through periodontal ligation with *P. gingivalis*, periodontitis could promote CD36-mediated fat deposition in the liver (45). Additionally, it has been shown that oral *P. gingivalis* infection can lead to notable TLR2-CD36/Sr-B2-dependent IL-1β release, resulting in increased foam cell formation and plaque development (46). Taken together, these findings suggested that oral *P. gingivalis* infection can promote CD36 fat deposition in the liver, affect lipid metabolism, increase the release of inflammatory factors and promote plaque enlargement. Further investigation suggested that targeting CD36 may be a feasible strategy for reducing the additional risk of atherosclerosis through factors that contribute to systemic inflammation, such as periodontal disease (47).

PPARs serve as fatty acid sensors, which regulate a number of pathways involved in lipid and glucose metabolism, as well as overall energy metabolism. LXRs are sterol sensors, which

predominantly regulate cholesterol, fatty acid and glucose homeostasis; these receptors can also inhibit the development of atherosclerosis (48). PPARγ, which is a key regulator of CD36, regulates lipid metabolism by activating LXRα and upregulating ABCA1 expression (49). However, the genes involved in lipid efflux reportedly downregulate PPARγ and LXRα during *P. gingivalis*-induced macrophage formation in foam cells. In the presence of LDL, this downregulation is dose-dependent (50). In the current study, the levels of PPARγ and LXRα in *P. gingivalis*-infected mice were determined, and it was revealed that LXRα levels were significantly lower in *ApoE*$^{-/-}$ infected group mice than those in in wild-type infected mice. Similarly, PPARγ levels were significantly lower in the *ApoE*$^{-/-}$ infected group than in the wild-type infected group. However, no significant difference in PPARγ levels was observed between the *ApoE*$^{-/-}$ control group and the *ApoE*$^{-/-}$ infected group. These findings suggested that *P. gingivalis* infection may further aggravate atherosclerosis by affecting the levels of PPARγ and LXRα. In addition, TLR4 signaling contributes to *P. gingivalis*-induced reduction in LXRα gene expression via the TRIF branch, whereas the IRF3 status affects *P. gingivalis*-induced LXRα gene expression in macrophages (51). These findings further confirmed that LXRα expression is downregulated in the inflammatory state. ABCA1 and ABCG1 are considered key proteins that mediate liver cholesterol output. The expression of these transporters is predominantly dependent on the activation of the PPARγ and LXRα transcription factors (52). In order to determine whether the expression levels of ABCA1/G1, downstream genes of PPARγ and LXRα, were also affected by *P. gingivalis*, the expression levels of ABCA1 and ABCG1 in mice were determined in the current study. It was revealed that, compared with those in the wild-type mice, the expression levels of ABCG1 in the liver of *P. gingivalis*-infected wild-type mice were increased; this upregulation may be a protective reaction of wild-type mice to a mild infection by *P. gingivalis*. High levels of PPARγ have been suggested to directly promote the expression of ABCG1, thereby enhancing the excretion of cholesterol in the liver (11). This finding was consistent with previous studies, which showed that treatment of THP-1-derived macrophages co-cultured with LDL with LPS from *P. gingivalis* could inhibit ABCG1 expression in a time- and concentration-dependent manner (26,53). Reduced ABCA1 and ABCG1 expression can mediate lipid accumulation. It has also been suggested that the activation of PPARγ facilitates cholesterol efflux mainly through ABCG1 but not through ABCA1 (54). However, compared with those in the uninfected *ApoE*$^{-/-}$ group, the expression levels of ABCA1 and ABCG1 were not significantly decreased in the *ApoE*$^{-/-}$ infection group. This may be related to the regulation of ABCA1 and ABCG1 by ILs in the inflammatory state; however, further experimental validation of this finding and inference is needed.

In conclusion, the present study revealed that oral *P. gingivalis* infection can exacerbate inflammatory responses and lipid metabolism disorders, further aggravating atherosclerosis. The PPARγ-LXRα-ABCA1/ABCG1 signaling pathway may serve a role in this process, although the specific interaction between the inflammatory response and lipid metabolism remains to be explored further.

Acknowledgements

Not applicable.

Funding

This research was funded by the National Natural Science Foundation of China (grant no. 82201080), the Hainan S&T Program (grant no. KJTP202561) and the Academic Enhancement Support Program of Hainan Medical University (grant no. XSTS2025027).

Availability of data and materials

The data generated in the present study may be requested from the corresponding author.

Authors' contributions

XJL and MY participated in the conception and design of the study, acquisition and analysis of data, and drafting of the manuscript. ZLG participated in the conceptualization and supervision of the study. WYL, QY, JZ, LHW and DS were involved in data collection and analysis. MZUS, WXX, YLD, MMZ and MWC participated in the experimental design and methodological optimization. XJL, MY, ZLG, WYL, QY, JZ, LHW, DS, MZUS, WXX, YLD, MMZ and MWC confirm the authenticity of all the raw data. All authors read and approved the final manuscript.

Ethics approval and consent to participate

This research protocol obtained full ethical clearance from the ethics committee of Hainan Medical University (approval no. HYLL-2021-121) and rigorously adhered to the relevant guidelines established by the National Institutes of Health.

Patient consent for publication

Not applicable.

Competing interests

The authors declare that they have no competing interests.

References

1. Hussain A, Ballantyne CM, Saeed A and Virani SS: Triglycerides and ASCVD risk reduction: Recent insights and future directions. Curr Atheroscler Rep 22: 25, 2020.
2. Mendoza MF, Anzelmo MA, Suan NM, Cuccia CS and Lavie CJ: More than just a toothache: Inflammatory mechanisms linking periodontal disease to cardiovascular disease and the protective impact of cardiorespiratory fitness. Biomedicines 13: 1512, 2025.
3. Tang Y, Qi Y, Chen Y, Wang YQ, Zhang C, Sun Y, Huang C and Zhang XZ: Erythrocyte-mimicking nanovesicle targeting porphyromonas gingivalis for periodontitis. ACS Nano 18: 21077-21090, 2024.
4. Ding C, Shen Z, Xu R, Liu Y, Xu M, Fan C, Hu D and Xing T: Exosomes derived from periodontitis induce hepatic steatosis through the SCD-1/AMPK signaling pathway. Biochim Biophys Acta Mol Basis Dis 1870: 167343, 2024.
5. Yuan Q, Dong YL and Guo ZL: Research progress on the intervention of *Porphyromonas gingivalis* in chronic obstructive pulmonary disease. J Hainan Med Univ 31: 229-240, 2025 (In Chinese).

6. Wu Q, Li Z, Zhang Y, Luo K, Xu X, Li J, Peng X and Zhou X: Cyclic di-AMP rescues porphyromonas gingivalis-aggravated atherosclerosis. J Dent Res 102: 785-794, 2023.
7. Schenkein HA, Papapanou PN, Genco R and Sanz M: Mechanisms underlying the association between periodontitis and atherosclerotic disease. Periodontol 2020, 83: 90-106, 2000.
8. Kim Y, Lee H, Park HJ, Kim MK, Kim YI, Kim HJ, Bae SK, Kim YJ and Bae MK: Hispidulin inhibits the vascular inflammation triggered by porphyromonas gingivalis lipopolysaccharide. Molecules 28: 6717, 2023.
9. He XW, Yu D, Li WL, Zheng Z, Lv CL, Li C, Liu P, Xu CQ, Hu XF and Jin XP: Anti-atherosclerotic potential of baicalin mediated by promoting cholesterol efflux from macrophages via the PPARγ-LXRα-ABCA1/ABCG1 pathway. Biomed Pharmacother 83: 257-264, 2016.
10. Chen H, Tan H, Wan J, Zeng Y, Wang J, Wang H and Lu X: PPAR-γ signaling in nonalcoholic fatty liver disease: Pathogenesis and therapeutic targets. Pharmacol Ther 245: 108391, 2023.
11. Matsuo M: ABCA1 and ABCG1 as potential therapeutic targets for the prevention of atherosclerosis. J Pharmacol Sci 148: 197-203, 2022.
12. Wang W, Zhang Y, Wang Z, Zhang J and Jia L: Ganoderma lucidum polysaccharides improve lipid metabolism against high-fat diet-induced dyslipidemia. J Ethnopharmacol 309: 116321, 2023.
13. Lockhart SM, Muso M, Zvetkova I, Lam BYH, Ferrari A, Schoenmakers E, Duckett K, Leslie J, Collins A, Romartínez-Alonso B, *et al*: Damaging mutations in liver X receptor-α are hepatotoxic and implicate cholesterol sensing in liver health. Nat Metab 6: 1922-1938, 2024.
14. Wang H, Yang Y, Sun X, Tian F, Guo S, Wang W, Tian Z, Jin H, Zhang Z and Tian Y: Sonodynamic therapy-induced foam cells apoptosisactivatesthephagocyticPPARγ-LXRα-ABCA1/ABCG1 pathway and promotes cholesterol efflux in advanced plaque. Theranostics 8: 4969-4984, 2018.
15. Song X, Yan G, Wang H and Lou D: Septin 4 activates PPARγ/LXRα signaling by upregulating ABCA1 and ABCG1 expression to inhibit the formation of THP-1 macrophage-derived foam cells. Exp Ther Med 22: 763, 2021.
16. Mahdavi-Roshan M, Salari A, Kheirkhah J and Ghorbani Z: The effects of probiotics on inflammation, endothelial dysfunction, and atherosclerosis progression: A mechanistic overview. Heart Lung Circ 31: e45-e71, 2022.
17. Litvinchuk A, Suh JH, Guo JL, Lin K, Davis SS, Bien-Ly N, Tycksen E, Tabor GT, Remolina Serrano J, Manis M, *et al*: Amelioration of Tau and ApoE4-linked glial lipid accumulation and neurodegeneration with an LXR agonist. Neuron 112: 384-403.e8, 2024.
18. Hofseth LJ: Getting rigorous with scientific rigor. Carcinogenesis 39: 21-25, 2018.
19. Xuan Y, Cai Y, Wang XX, Shi Q, Qiu LX and Luan QX: Effect of Porphyromonas gingivalis infection on atherosclerosis in apolipoprotein-E knockout mice. Beijing Da Xue Xue Bao Yi Xue Ban 52: 743-749, 2020.
20. Miyamoto T, Yumoto H, Takahashi Y, Davey M, Gibson FC III and Genco CA: Pathogen-accelerated atherosclerosis occurs early after exposure and can be prevented via immunization. Infect Immun 74: 1376-1380, 2006.
21. Chatterjee S: Endothelial Mechanotransduction, redox signaling and the regulation of vascular inflammatory pathways. Front Physiol 9: 524, 2018.
22. Livak KJ and Schmittgen TD: Analysis of relative gene expression data using real-time quantitative PCR and the 2(-Delta Delta C(T)) Method. Methods 25: 402-408, 2001.
23. Ridker PM and Rane M: Interleukin-6 signaling and anti-interleukin-6 therapeutics in cardiovascular disease. Circ Res 128: 1728-1746, 2021.
24. Nakagawa K and Nakashima Y: Pathologic intimal thickening in human atherosclerosis is formed by extracellular accumulation of plasma-derived lipids and dispersion of intimal smooth muscle cells. Atherosclerosis 274: 235-242, 2018.
25. Xie M, Tang Q, Nie J, Zhang C, Zhou X, Yu S, Sun J, Cheng X, Dong N, Hu Y and Chen L: BMAL1-Downregulation aggravates porphyromonas gingivalis-induced atherosclerosis by encouraging oxidative stress. Circ Res 126: e15-e29, 2020.
26. Zou Y, Huang Y, Liu S, Yang J, Zheng W, Deng Y, Zhang M, Yan Z and Xie H: Periodontopathic microbiota and atherosclerosis: Roles of TLR-mediated inflammation response. Oxid Med Cell Longev 2022: 9611362, 2022.
27. Huang X, Xie M, Lu X, Mei F, Song W, Liu Y and Chen L: The roles of periodontal bacteria in atherosclerosis. Int J Mol Sci 24: 12861, 2023.
28. Lin XJ, Yuan Q, Zhou J, Dong YL, Sunchuri D and Guo ZL: Cellular senescence: A new perspective on the suppression of periodontitis (Review). Mol Med Rep 30: 238, 2024.
29. Hou L, Feng X, Zhu Z, Mi Y, He Q, Yin K and Zhao G: IGFBPL1 inhibits macrophage lipid accumulation by enhancing the activation of IGR1R/LXRα/ABCG1 pathway. Aging (Albany NY) 15: 14791-14802, 2023.
30. Kuula H, Salo T, Pirilä E, Tuomainen AM, Jauhiainen M, Uitto VJ, Tjäderhane L, Pussinen PJ and Sorsa T: Local and systemic responses in matrix metalloproteinase 8-deficient mice during Porphyromonas gingivalis-induced periodontitis. Infect Immun 77: 850-859, 2009.
31. Wacker M, Ball A, Beer HD, Schmitz I, Borucki K, Azizzadeh F, Scherner M, Awad G, Wippermann J and Veluswamy P: Immunophenotyping of monocyte migration markers and therapeutic effects of selenium on IL-6 and IL-1β cytokine axes of blood mononuclear cells in preoperative and postoperative coronary artery disease patients. Int J Mol Sci 24: 7198, 2023.
32. Ledard N, Liboz A, Blondeau B, Babiak M, Moulin C, Vallin B, Guillas I, Mateo V, Jumeau C, Blirando K, *et al*: Slug, a cancer-related transcription factor, is involved in vascular smooth muscle cell transdifferentiation induced by platelet-derived growth factor-BB during atherosclerosis. J Am Heart Assoc 9: e014276, 2020.
33. Ruan Q, Guan P, Qi W, Li J, Xi M, Xiao L, Zhong S, Ma D and Ni J: Porphyromonas gingivalis regulates atherosclerosis through an immune pathway. Front Immunol 14: 1103592, 2023.
34. Mendez-Sanchez N, Cruz-Ramon VC, Ramirez-Perez OL, Hwang JP, Barranco-Fragoso B and Cordova-Gallardo J: New aspects of lipotoxicity in nonalcoholic steatohepatitis. Int J Mol Sci 19: 2034, 2018.
35. Liu C, Schönke M, Zhou E, Li Z, Kooijman S, Boon MR, Larsson M, Wallenius K, Dekker N, Barlind L, *et al*: Pharmacological treatment with FGF21 strongly improves plasma cholesterol metabolism to reduce atherosclerosis. Cardiovasc Res 118: 489-502, 2022.
36. Zhou P, Shen Y, Wang L, Cao Z, Feng W, Liu J, Wang L, Meng P, Yang J, Xu WY and Gao P: Association between carotid intima media thickness and small dense low-density lipoprotein cholesterol in acute ischaemic stroke. Lipids Health Dis 19: 177, 2020.
37. Canbay E, Canda E, Yazıcı H, Kasıkcı GK, Durmaz B, Copur O, Tahhan B, Düzgün D, Koru ZE, Sezer E, *et al*: Determination of selected oxysterol levels, oxidative stress, and macrophage activation indicators in children and adolescents with familial hypercholesterolemia. Lipids Health Dis 23: 374, 2024.
38. Robinett NG, Culbertson EM, Peterson RL, Sanchez H, Andes DR, Nett JE and Culotta VC: Exploiting the vulnerable active site of a copper-only superoxide dismutase to disrupt fungal pathogenesis. J Biol Chem 294: 2700-2713, 2019.
39. Schatzman SS, Peterson RL, Teka M, He B, Cabelli DE, Cormack BP and Culotta VC: Copper-only superoxide dismutase enzymes and iron starvation stress in Candida fungal pathogens. J Biol Chem 295: 570-583, 2020.
40. Calcaterra V, Verduci E, Cena H, Magenes VC, Todisco CF, Tenuta E, Gregorio C, De Giuseppe R, Bosetti A, Di Profio E and Zuccotti G: Polycystic ovary syndrome in insulin-resistant adolescents with obesity: The role of nutrition therapy and food supplements as a strategy to protect fertility. Nutrients 13: 1848, 2021.
41. Al-Ahmadi W, Webberley TS, Joseph A, Harris F, Chan YH, Alotibi R, Williams JO, Alahmadi A, Decker T, Hughes TR and Ramji DP: Pro-atherogenic actions of signal transducer and activator of transcription 1 serine 727 phosphorylation in LDL receptor deficient mice via modulation of plaque inflammation. FASEB J 35: e21892, 2021.
42. Zhang F, Liu P, He Z, Zhang L, He X, Liu F and Qi J: Crocin ameliorates atherosclerosis by promoting the reverse cholesterol transport and inhibiting the foam cell formation via regulating PPARγ/LXR-α. Cell Cycle 21: 202-218, 2022.
43. Huang R, Pang Q, Zheng L, Lin J, Li H, Wan L and Wang T: Cholesterol metabolism: physiological versus pathological aspects in intracerebral hemorrhage. Neural Regen Res 20: 1015-1030, 2025.
44. Wang H, Wang L, Liu Y, Men W, Hao W, Fang C, Li C and Zhang L: Plasma levels of CD36 and glutathione as biomarkers for ruptured intracranial aneurysm. Open Life Sci 18: 20220757, 2023.

45. Ahn JS, Yang JW, Oh SJ, Shin YY, Kang MJ, Park HR, Seo Y and Kim HS: Porphyromonas gingivalis exacerbates the progression of fatty liver disease via CD36-PPARgamma pathway. BMB Rep 54: 323-328, 2021.
46. Kim D, Choi H, Oh H, Lee J, Hwang Y and Kang SS: Mutanolysin-Digested Peptidoglycan of lactobacillus reuteri promotes the inhibition of porphyromonas gingivalis lipopolysaccharide-induced inflammatory responses through the regulation of signaling cascades via TLR4 suppression. Int J Mol Sci 25: 42, 2023.
47. Rekhi UR, Catunda RQ, Alexiou M, Sharma M, Fong A and Febbraio M: Impact of a CD36 inhibitor on Porphyromonas gingivalis mediated atherosclerosis. Arch Oral Biol 126: 105129, 2021.
48. Cariello M, Piccinin E and Moschetta A: Transcriptional regulation of metabolic pathways via lipid-sensing nuclear receptors PPARs, FXR, and LXR in NASH. Cell Mol Gastroenterol Hepatol 11: 1519-1539, 2021.
49. Afzoon S, Amiri MA, Mohebbi M, Hamedani S and Farshidfar N: A systematic review of the impact of Porphyromonas gingivalis on foam cell formation: Implications for the role of periodontitis in atherosclerosis. BMC Oral Health 23: 481, 2023.
50. Huang N, Shaik-Dasthagirisaheb YB, LaValley MP and Gibson FC III: Liver X receptors contribute to periodontal pathogen-elicited inflammation and oral bone loss. Mol Oral Microbiol 30: 438-450, 2015.
51. Mao M, Deng Y, Wang L, Zhao G, Qi R, Gong H, Shen T, Xu Y, Liu D and Chen B: Chronic unpredictable mild stress promotes atherosclerosis via adipose tissue dysfunction in ApoE(-/-) mice. PeerJ 11: e16029, 2023.
52. Javadifar A, Rastgoo S, Banach M, Jamialahmadi T, Johnston TP and Sahebkar A: Foam cells as therapeutic targets in atherosclerosis with a focus on the regulatory roles of non-coding RNAs. Int J Mol Sci 22: 2529, 2021.
53. Li XY, Wang C, Xiang XR, Chen FC, Yang CM and Wu J: Porphyromonas gingivalis lipopolysaccharide increases lipid accumulation by affecting CD36 and ATP-binding cassette transporter A1 in macrophages. Oncol Rep 30: 1329-1336, 2013.
54. Shen X, Zhang S, Guo Z, Xing D and Chen W: The crosstalk of ABCA1 and ANXA1: A potential mechanism for protection against atherosclerosis. Mol Med 26: 84, 2020.